THE JOURNAL OF PHYSICAL CHEMISTRY C

ARTICLE

pubs.acs.org/JPCC

Influence of the Organic Ligand Functionalization on the Breathing of the Porous Iron Terephthalate Metal Organic Framework Type Material upon Hydrocarbon Adsorption

Naseem A. Ramsahye,[†] Thuy Khuong Trung,[†] Sandrine Bourrelly,[§] Qingyuan Yang,[†,⊥] Thomas Devic,[‡] Guillaume Maurin,[†] Patricia Horcajada,[‡] Philip L. Llewellyn,[§] Pascal Yot,[†] Christian Serre,[‡] Yaroslav Filinchuk,[∥] François Fajula,[†] Gérard Férey,[‡] and Philippe Trens*[,†]

[†]ICGM, UMR CNRS 5253, ENSCM, 8 rue de l'Ecole Normale, 34296 Montpellier cedex 5, France

[‡]Lavoisier Institute, UMR CNRS 8180, UVSQ, 45 avenue des Etats-Unis, 78035 Versailles, France

[§]Laboratory of Chemistry of Provence (UMR 6264), Universities Aix-Marseille I, II, and III — CNRS, 13397 Marseille cedex 20, France

[∥]SNBL at ESRF, rue Jules Horowitz, 38043 Grenoble, France

[⊥]Department of Chemical Engineering, Key Lab for Nanomaterials, Ministry of Education, Beijing University of Chemical Technology, Beijing 100029, China

Supporting Information

ABSTRACT: A combination of manometry, X-ray powder diffraction (XRPD), and molecular modeling has been used to show that the functionalization of the flexible MIL-53(Fe)-X materials (MIL stands for Materials of the Lavoisier Institute; X = CH_3, Cl, Br, NH_2) modifies the adsorption process of normal alkanes, by facilitating pores filling as compared to that of the nonmodified MIL-53(Fe) analogue. The adsorption isotherms show that these materials undergo steps at pressures specific for each guest and functional group, associated with structural transitions as corroborated by the simulated isotherms and XRPD data. With the exception of methane, a transition from the closed pore form to the large pore form occurs through one intermediate pore form upon adsorption, thus differing from the case of the nonmodified MIL-53(Fe) where two intermediate pore forms are observed. The transitions are governed by a combination of factors, including energetic, kinetic, and steric aspects with, however, transition pressures becoming increasingly lower with increasing number of C atoms on the adsorbate. This can be rationalized in terms of increased host−guest interactions. In addition, molecular modeling gives insights into the adsorption mechanism, in terms of the arrangement of the molecules within the pores, allowing the rationalization of the different amounts of *n*-nonane adsorbed in relation to the other molecules. Finally, the arrangement of the molecules within the pores also plays a role in the kinetics of the adsorption process, which shows that the C6 (*n*-hexane) molecules require more time to reach a state of static equilibrium than the C9 (*n*-nonane) molecules, due to their greater degree of freedom resulting from their alignment along the pores.

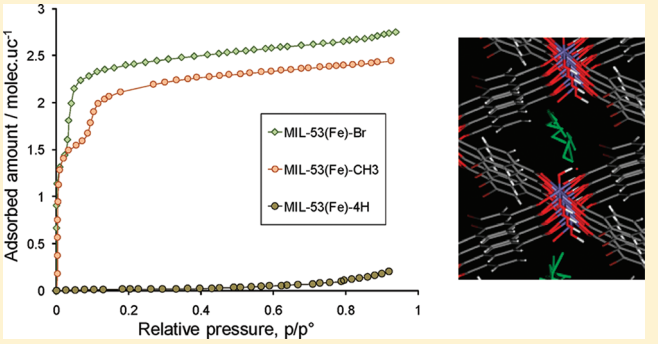

INTRODUCTION

Metal organic frameworks (MOFs) are hybrid porous materials that have emerged over the last decades. They are built up of metal oxides polyhedra connected by organic linkers to form a porous hybrid network and are currently very topical due to their interesting adsorption capacity, separation selectivity, catalytic behavior, or biomedical applications.[1−4]

Some of these porous materials are flexible, being able to reversibly and selectively increase their pore volume from 30% to 230% depending on the structures under consideration,[5−8] and the nature of the adsorbates present within the pores. This type of structural change in the MIL-53 (M = Al, Cr, Fe) series of solids is now a well-documented phenomenon. These metal(III) terephthalates are built up from chains of μ_2-OH corner-sharing $M(OH)_2O_4$ octahedra connected by the linear dicarboxylate linkers to define one-dimensional diamond-shaped pores. In the case of MIL-53(Al, Cr), the structural flexibility involves a switching between two different pore forms (the "breathing effect"), termed the narrow pore and the large pore, upon adsorption of molecules such as CO_2,[9−12] H_2O,[8,13] and *n*-alkanes.[14,15] Previous molecular modeling work has established that such a structural switching is mainly governed by a critical interplay between the

Received: June 8, 2011
Revised: August 14, 2011
Published: August 16, 2011

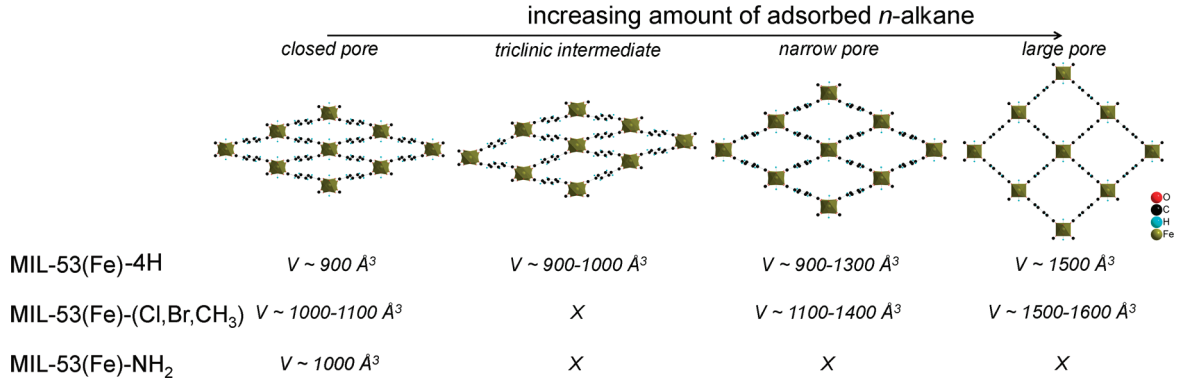

Figure 1. Structural transition observed upon increasing adsorption of *n*-alkanes within the nonmodified MIL-53(Fe) and modified MIL-53(Fe)-X (X = Cl, Br, CH_3, NH_2) solids. The unit-cell volumes (and thus the pore opening) of both the intermediate and the narrow pore forms are dependent on the nature of the guest, whereas the large pore form is almost insensitive.

host and the guest molecules, which induce a displacive type transition.[16] For CO_2 and H_2O, interactions with the μ_2-OH groups or oxygen from the carboxylates on the framework have been shown to play a crucial role in the breathing effect.[9,17] Interestingly, breathing requires an adsorption enthalpy exceeding an energy barrier.[12,18,19] Thus, nonspecific adsorbate/adsorbent interactions such as van der Waals type interactions that occur upon normal alkane adsorption can also induce such a spectacular phenomenon.[15,20] Note also that such transition, from a large pore form to closed pore form, was observed by simply cooling the activated (i.e., empty pores) MIL-53(Al) solid.[21] A recent computational study has shown that the interactions between the π systems of the organic linkers play a role in stabilizing the closed pore form of MIL-53(Al).[22] It raises the concept that the breathing is possible as long as a certain amount of stress is applied to the structure.[23,24] The breathing effect in the case of MIL-53(Fe) is more complex, involving three structural transitions.[14] Its activated form exhibits closed pores, regardless of the applied temperature.[25] Upon adsorption of gases, it passes through two intermediate structures, for example, a triclinic intermediate 1 and a monoclinic intermediate 2 phase, the latter corresponding to the narrow pore form of the (Al, Cr) analogues, and subsequently reopens to the large pore form, as shown in Figure 1. This has been demonstrated for this material during a study of the desorption of water[25,26] as well as in recent work on the adsorption of short gaseous linear alkanes.[14,26] The behavior of MIL-53 thus greatly depends on the nature of the metal ion present in the framework, and such information could be useful in designing flexible materials for specific adsorption purposes.

A second way of tuning the adsorption properties of a MOF consists of functionalizing organic linkers with different chemical groups, to adjust properties such as polarizability, acidity, and pore size, and in turn control both the adsorption capacity and the selectivity. So far, consequences of functionalization have been reported for adsorption[27,28] and catalysis.[29] However, only a few studies have dealt with adsorption in flexible functionalized MOFs.[30−34]

Recently, some of us have reported a series of modified MIL-53(Fe) solids, using functional groups such as Br, Cl, CH_3, NH_2, and others.[35] The resulting structures are initially in a closed pore configuration prior to adsorption with evidence of intramolecular H-bonds between the μ_2-OH group and polar substituent or interactions between the linkers facing each other that favor the pore closure. Therefore, for adsorption to occur, these H-bonds would have to be broken or at least loosened, allowing the expansion of the pores. Nevertheless, other parameters such as the relative stabilities of the different pore forms and the steric hindrance of the substituents might affect the breathing. The liquid-phase adsorption studies performed in this work show that polar solvent molecules that sufficiently interact with the framework render the structures flexible. However, the behavior of modified MIL-53(Fe) MOFs upon the adsorption of nonpolar molecules has not been detailed.

We report here the adsorption of linear hydrocarbons, from methane to *n*-nonane series, labeled C1, C2, C3, etc., in the nonmodified MIL-53(Fe) labeled as MIL-53(Fe)-4H, as well as in different modified MIL-53(Fe)-X materials (X = Br, Cl, CH_3, NH_2) at ambient temperature, using techniques such as manometry, in situ and ex situ X-ray powder diffraction (XRPD), and molecular modeling. These guest molecules are nonpolar and interact with the framework only through van der Waals type, allowing the study of the physical-mechanical properties of these solids without the presence of any specific interactions between the adsorbate and the framework.

EXPERIMENTAL DETAILS

Synthesis and Activation. MIL-53(Fe)-4H and MIL-53-(Fe)-Cl, Br, CH_3, NH_2 were prepared and activated according to the reported procedures.[14,35]

Adsorption of C1−C3. *Adsorption Gravimetry.* The adsorption isotherms were measured at 303 K and at pressures up to 50 bar using a commercial gravimetric adsorption device (Rubotherm Präzisionsmeßtechnik GmbH).[36] A step by step gas introduction mode was used. Approximately 1 g of sample was used for these experiments. Prior to each experiment, the sample was outgassed in situ at 200 °C for 16 h under primary vacuum (around 10^{-3} bar). Equilibrium was assumed when the variation of weight remains below 0.03% for 20 min. In this apparatus, the variation in sample weight and gas density can be measured consequently. The latter is obtained using a titanium sinker of known mass and volume and thus allows a direct correction of the buoyancy effect.[37]

Adsorption of C4. *Adsorption Manometry.* Because of the slow kinetics of the *n*-butane adsorption, we were not totally confident in the adsorption isotherms obtained with the automatic gravimetric adsorption device. Thus, to ensure the adsorption equilibrium for each dose of gas on the functionalized

Table 1. Unit-Cells of the Modified MIL-53(Fe)-Cl Loaded with Alkanes

gas	T (K)	P_{XRD} (bar)	space group	a	b	c	β	V	form	P^d (bar)	n ads^d (molec uc^{-1})
CH_4[a]	303	0	$C2/c$	20.165(1)	7.4947(7)	6.9196(4)	106.041(6)	1005.2(1)	cp	$0 < P < 19.98$	$n < 0.5$
		38.7	$C2/c$	20.085(2)	8.9947(7)	6.9250(5)	108.251(8)	1188.1(2)	np	$24.96 < P < 40.0$	$2 < n < 2.5$
C_2H_6[a]	303	0	$C2/c$	20.165(1)	7.5049(7)	6.9173(4)	106.069(5)	1005.9(1)	cp	$0 < P < 1.45$	$n < 0.5$
		5.2	$C2/c$	19.977(1)	9.3122(6)	6.9297(4)	108.394(5)	1223.3(1)	np	$1.95 < P < 15$	$2 < n < 2.5$
		36.3	$C2/c$	19.986(4)	9.622(2)	6.935(1)	108.35(2)	1265.9(4)	np		
			$Imcm$	16.772(1)	13.582(1)	6.9476(5)		1582.6(2)	lp	19.96 < P	$4.5 < n$
C_3H_8[a]	303	0	$C2/c$	20.112(4)	7.424(2)	6.898(2)	105.89(1)	990.5(4)	cp	$0 < P < 0.15$	
		0.92	$C2/c$	19.729(3)	10.116(1)	6.9140(8)	109.02(2)	1304.5(3)	np	$0.35 < P < 2.15$	$2 < n < 2.5$
		8	$Imcm$	16.8891(8)	13.2251(8)	6.9264(3)		1547.1(1)	lp	$3.9 < P < 8.0$	$3.5 < n < 4.2$
C_4H_{10}[a]	303	0	$C2/c$	20.165(1)	7.4933(8)	6.9179(5)	106.038(6)	1004.6(1)	cp	$P < 0.05$	
		0.56	$C2/c$	19.661(6)	10.607(3)	6.9526(9)	109.46(2)	1367.1 (6)	np	$0.03 < P < 0.5$	$1.5 < n < 2.3$
		2.1	$Imcm$	16.791(1)	13.542(1)	6.9459(5)		1579.4(2)	lp	$0.9 < P < 2.25$	$3.0 < n < 3.5$
n-C_6H_{14}[b]	~300	1 (RP)	$Imcm$	17.7774(7)	11.8426(6)	6.9296(2)		1458.9(1)	lp	$7.0 \times 10^{-3} < P < 0.34$	$1.8 < n < 2.1$
	~370		$Imcm$	18.3382(8)	10.8086(8)	6.9299(4)		1373.6(1)	np		
	~530		$C2/c$	20.149(1)	8.0739(6)	6.9069(3)	107.177(5)	1073.5(1)	cp		
n-C_6H_{14}[c]	303	0.016	$C2/c$	19.706(1)	10.1514(5)	6.9222(3)	109.051(4)	1308.9(1)	np		
n-C_7H_{16}[c]	303	0.006	$C2/c$	20.150(1)	7.4809(7)	6.9034(5)	105.937(6)	1000.6(1)	cp		
			$C2/c$	19.643(2)	10.146(1)	6.9308(9)	108.70(1)	1308.3(3)	np		
n-C_8H_{18}[c]	303	0.002	$C2/c$	20.154(1)	7.4114(6)	6.9105(5)	106.002(6)	992.2(1)	cp		
			$C2/c$	19.717(2)	10.0687(8)	6.9271(5)	108.876(7)	1301.3(2)	np		
n-C_9H_{20}[b]	~310	1 (RP)	$Pnam$	17.2580(3)	12.5722(2)	6.9371(1)		1505.15(4)	lp	$3.0 \times 10^{-4} < P < 0.013$	$0.8 < n < 1.2$
	~500		$Imcm$	18.188(3)	10.956(3)	6.911(1)		1377.1(4)	np		
	~570		$C2/c$	19.971(5)	8.062(2)	6.884(2)	106.80(2)	1061.1(5)	cp		

[a] In situ experiments at fixed temperature. [b] In situ experiments at variable temperature (RP = room pressure). [c] Ex situ experiments. [d] From gravimetry or/manometric measurements at 303 K.

MIL-53(Fe), the C4 adsorption experiments were performed manually, step by step, with a homemade manometric device (with a 0−5 bar pressure gauge). The equilibrium time depends on experimental parameters such as sample mass, amount of gas injected, and the pressure domain where adsorption occurs. This is especially the case during the adsorption steps where structure transitions occur. For C1−C3, the equilibrium time is around 1−1.5 h, whereas during C4 adsorption, the equilibrium time is around 4−5 h.

Adsorption of C6−C9. In the case of the longer chain alkanes, from C6 to C9, vapor adsorption/desorption experiments have been performed with a homemade apparatus already described elsewhere.[38] This setup is based on manometric measurements (with two capacitive pressure gauges (0−10 mbar and 0−1000 mbar)). The sample cell can be disconnected from the system to undergo a thermal treatment up to 250 °C under a vacuum of 10^{-3} mbar. The thermal stability of the samples was tested prior to the thermal treatment by thermogravimetry. The *n*-alkanes used as adsorbates (provided by Aldrich, purity >99.9%) were outgassed and stored over activated 3 Å molecular sieve. This setup allows the choice of the pressure of the adsorbate to be introduced. The amount of sample used is usually around 150 mg. Vapor adsorption was performed at 313 K, each sorption experiment being performed with fresh samples to be sure of the initial state of activation of the samples. A duration of 300 s at the same pressure in the sample cell was chosen as criterium for the thermodynamic equilibrium.[38] Longer times of equilibration gave the same sorption isotherms. Depending on the relative pressure, and therefore the sorption process, different times of adsorption could be observed (see later).

X-ray Diffraction Studies. X-ray powder diffraction (XRPD) patterns were collected at the BM01A station at the Swiss Norwegian Beamline of the European Synchrotron Radiation Facility (Grenoble, France). Depending on the *n*-alkane length, different setups were employed.

C1−C4. For in situ experiments, the powdered sample was introduced in a 1 mm quartz capillary and connected to a homemade gas dosing system.[14] Prior to the experiments, the sample was outgassed under vacuum (pressure of about 10^{-3} mbar) at 473 K for a few hours. The temperature was then adjusted to 303 K, and doses of gas mixtures were introduced. XRPD were collected using a MAR345 imaging plate with a sample-to-detector distance of 400 mm (depending on the experiment, λ = 0.699765, 0.7004, 0.694018, or 0.7183 Å). X-ray powder diffractograms were collected 1 min after the gas introduction, with an acquisition time of 30−60 s (rotation rate $1° s^{-1}$). New X-ray powder diffraction patterns were recorded at the same pressure every 5 min, and equilibrium (at a given pressure) was assumed when no change was observed between the successive patterns. To assess the effect of the functionalization on the kinetic of adsorption, another set of experiments was performed. Starting from the same activated solids, C4 was introduced at the highest pressure available (2.6−3.1 bar at 303 K), to reach the large pore form at the equilibrium. The patterns were collected every 60 s until no more change occurred, thus allowing one to follow the transition from a kinetic point of view.

C6−C9. For ex situ experiments, dehydrated samples were loaded in a glass capillary (diameter 0.7 mm) and heated under vacuum (473 K) for few hours. A dose of *n*-hexane or *n*-nonane

Table 2. Unit-Cells of the Modified MIL-53(Fe)-Br Loaded with Alkanes

gas	T (K)	P (bar)	space group	a	b	c	β	V	form	P^d (bar)	n ads^d (molec uc^{-1})
CH_4[a]	303	0	$C2/c$	20.1605(7)	8.0258(3)	6.9149(2)	107.091(2)	1069.45(6)	cp	$P < 1.0$	$n < 0.5$
		40.3	$C2/c$	20.2140(5)	8.9474(3)	6.9175(2)	109.126(2)	1182.06(6)	np	$14.9 < P < 40.0$	$2 < n < 3$
C_2H_6[a]	303	0	$C2/c$	20.1672(7)	8.0267(3)	6.9157(2)	107.079(2)	1070.13(6)	cp	$P > 0.35$	
		12.2	$C2/c$	20.0654(6)	9.2865(3)	6.9334(2)	108.935(3)	1222.04(7)	np	$3.0 < P < 17.0$	$2.2 < n < 2.5$
		37.7	$Imcm$	16.5533(5)	13.7082(4)	6.9310(2)		1572.76(8)	lp	$24.3 < P$	$3.6 < n$
C_3H_8[a]	303	0	$C2/c$	20.1638(6)	7.9958(3)	6.9138(2)	106.947(3)	1066.28(6)	cp	$P < 0.05$	
		1.1	$C2/c$	20.033(1)	9.7675(5)	6.9300(3)	110.213(6)	1272.5(1)	np	$0.32 < P < 2.29$	$1.9 < n < 2.1$
		8.2	$Imcm$	16.6484(7)	13.5529(8)	6.9260(2)		1562.7(1)	lp	$0.74 < P < 1.83$	$3.0 < n < 3.8$
n-C_4H_{10}[a]	303	0	$C2/c$	20.169(2)	8.018(1)	6.9158(8)	107.18(1)	1069.0(2)	cp	$P < 1 \times 10^{-3}$	
		0.7	$C2/c$	19.994(1)	9.8793(6)	6.934(4)	110.30(8)	1284.7(1)	np	$0.04 < P < 0.26$	$1.6 < n < 1.9$
	263	0.7	$Imcm$	16.4966(5)	13.7347(5)	6.9256(2)		1569.19(9)	lp		
n-C_6H_{14}[b]	~310	1 (RP)	$Imcm$	16.6968(4)	13.4970(5)	6.9286(2)		1561.42(8)	lp	$0.033 < P < 0.35$	$2.4 < n < 2.8$
	~460		$Imcm$	17.4038(7)	12.4456(7)	6.9200(3)		1498.9(1)	np		
	~560		$C2/c$	20.1374(6)	8.6933(5)	6.9123(2)	108.283(2)	1148.99(8)	cp		
n-C_6H_{14}[c]	303	0.025	$Imcm$	18.7508(9)	9.8755(5)	6.9307(3)		1283.4(1)	np	$7.9 \times 10^{-4} < P < 0.012$	$1.1 < n < 1.4$
		0.032	$C2/c$	20.138(2)	8.0295(9)	6.9182(5)	107.062(9)	1069.4(2)	cp		
			$Imcm$	18.8829(9)	9.5501(5)	6.9302(6)		1249.7(1)	np		
n-C_7H_{16}[c]	303	0.008	$C2/c$	20.162(1)	8.0318(7)	6.9163(6)	107.218(9)	1069.8(1)	cp		
			$Imcm$	18.8497(9)	9.6340(4)	6.9294(5)		1258.4(1)	np	$4.3 \times 10^{-4} < P < 4.6 \times 10^{-3}$	$1.1 < n < 1.3$
n-C_9H_{20}[b]	~340	1 (RP)	$Imcm$	17.1234(8)	12.8784(8)	6.9322(2)		1528.7(1)	lp	$3.1 \times 10^{-3} < P < 0.014$	$1.1 < n < 1.3$
	~390		$Imcm$	17.3558(7)	12.5476(7)	6.9334(3)		1509.9(1)	lp		
	~410		$Imcm$	18.339(1)	10.828(1)	6.9324(4)		1376.6(2)	np		
	~560		$C2/c$	20.1512(7)	8.6192(5)	6.9136(2)	108.158(3)	1141.01(8)	cp		

[a] In situ experiments at fixed temperature. [b] In situ experiments at variable temperature (RP = room pressure). [c] Ex situ experiments. [d] From gravimetry or/manometric measurements at 303 K.

Table 3. Unit-Cells of the Modified MIL-53(Fe)-CH_3 Loaded with Alkanes

gas	T (K)	P (bar)	space group	a	b	c	β	V	form	P^c (bar)	n ads^c (molec uc^{-1})
CH_4[a]	303	0	$C2/c$	20.086(1)	7.686(5)	6.8834(4)	106.150(5)	1020.8(1)	cp	$P < 10.10$	$n < 0.5$
		21.7	$C2/c$	20.155(2)	7.949(2)	6.8935(7)	106.65(1)	1058.2(3)	cp		
		42.0	$C2/c$	20.01(1)	8.752(4)	6.862(3)	107.31(4)	1147(1)	np	$19.9 < P < 40.0$	$1.9 < n < 2.5$
C_2H_6[a]	303	0	$C2/c$	20.023(2)	7.864(1)	6.8896(6)	106.221(9)	1041.7(2)	cp	$P < 0.95$	
		7.9	$C2/c$	19.941(3)	9.175(1)	6.905(1)	107.95(2)	1201.8(3)	np	$1.90 < P < 9.95$	$1.9 < n < 2.3$
		38.2	$C2/c$	19.920(4)	9.365(1)	6.918(2)	108.59(2)	1223.3(4)	np		
			$Imcm$	16.4812(9)	13.7160(9)	6.9223(2)		1564.8(1)	lp	$13.95 < P < 29.95$	$4.8 < n < 5.2$
C_3H_8[a]	303	0	$C2/c$	20.087(1)	7.7278(8)	6.8837(5)	106.272(6)	1025.7(1)	cp	$P < 0.23$	
		1.2	$C2/c$	19.53	10.09	6.88	108.3	1288	np	$0.95 < P < 1.75$	$2.4 < n < 2.7$
n-C_6H_{14}[b]	303	0.029	$C2/c$	20.104(2)	7.7777(8)	6.8914(8)	106.66(1)	1032.3(2)	cp		
			$C2/c$	19.530(2)	10.073(1)	6.8960(6)	108.380(8)	1287.5(2)	np	$3.2 \times 10^{-3} < P < 2.6 \times 10^{-2}$	$1.3 < n < 1.6$
	303	0.143	$Imcm$	16.8273(8)	13.2759(5)	6.9180(3)		1545.5(1)	lp	$0.049 < P < 0.34$	$2.0 < n < 2.4$
n-C_9H_{20}[b]	303	0.001	$C2/c$	20.079(2)	7.7959(8)	6.8865′5)	106.401(7)	1034.1(2)	cp		
			$C2/c$	19.483(3)	10.239(1)	6.902(1)	108.28(2)	1307.3(3)	np	$5.1 \times 10^{-4} < P < 8.1 \times 10^{-3}$	$0.7 < n < 0.8$
	303	0.009	$C2/c$	19.3682(9)	10.5316(5)	6.9098(3)	108.420(4)	1337.2(1)	np		

[a] In situ experiments at fixed temperature. [b] Ex situ experiments. [c] From gravimetry or/manometric measurements at 303 K.

was introduced in the capillary to reach a given $p/p°$ value at 303 K; the capillary was then flame-sealed and measured at 303 K.

For in situ experiments, dehydrated solids suspended in n-alkane were introduced in an open glass capillary (diameter 1 mm); the capillary was then heated to 650 K at about 150 K min^{-1}. Although this experiment is performed out of equilibrium, it allowed diffractograms of good quality to be measured for some structures, which are difficult to observe in their pure form by ex situ experiments.

The data were integrated using the Fit2D program (Dr. A. Hammersley, ESRF) and a calibration measurement of a NIST LaB6 standard sample. The patterns were indexed using the Dicvol software.[39] Le Bail fits were then performed with Fullprof2k and Winplotr software package.[40,41]

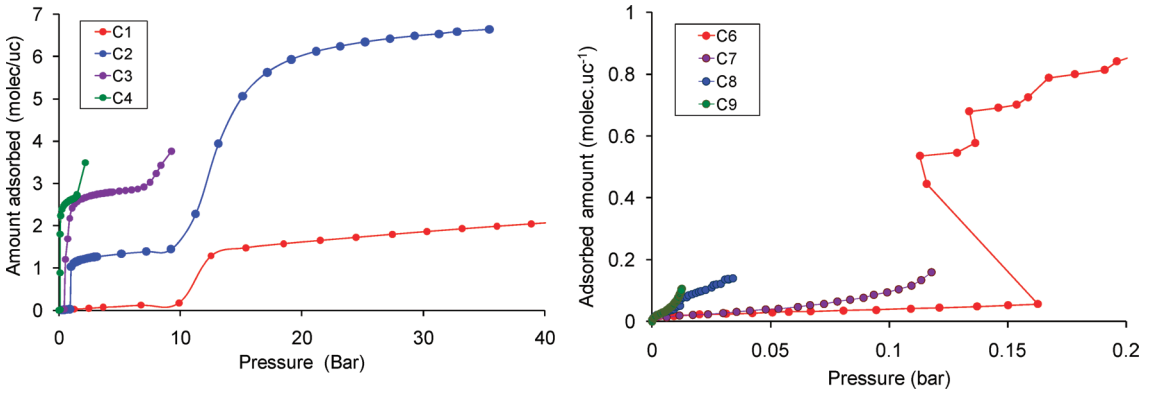

Figure 2. Isotherms for C1−C4 gases (left) at 303 K and C6−C9 vapors at 313 K (right) adsorbed on MIL-53(Fe)-4H.

The resulting unit-cell parameters are summarized in Tables 1−3.

Molecular Simulations. *Computational-Assisted Structure Determination.* The initial models for the narrow (NP) and the large (LP) pore forms of the bare MIL-53(Fe) were taken from our previous work. The starting configurations for each modified MIL-53(Fe) structure in the presence of all of the investigated *n*-alkanes were then built by (i) substituting the phenyl rings by the corresponding terephthalate linkers, and (ii) imposing the unit-cell parameters obtained from the XRPD refinement (see Tables 1−3) for both LP and NP forms in the presence of each alkane. Further, for each modified MIL-53(Fe), several initial models were generated corresponding to different positions of the modified terephthalate linkers over the four phenyl rings available per unit-cell. All of these models were then energy minimized in the space group *P*1, by maintaining the cell parameters fixed, and using the Universal force field (UFF)[42] and charges calculated from the electronegativity equalization method as implemented in the Materials Studio software.[43] Such a strategy has been successfully employed to construct plausible structure of various MILs including the dry modified MIL-53-Fe series and other related MOFs.[35,44] All of the details of the procedure employed can be found elsewhere.[14] The optimized structures with the lowest energies were selected for each of these modified materials. All of the energy minimizations converged to provide the plausible crystallographic structures for each form of MIL-53(Fe) experimentally detected in the presence of the various alkanes.

Grand Canonical Monte Carlo Simulations. On the basis of the above optimized structures, the configurational-bias grand canonical Monte Carlo (CB-GCMC) technique was further performed to predict the adsorption isotherms of the different *n*-alkanes covering from C1 to C4 and C6 to C9 at 303 and 313 K, respectively, using the simulation code CADSS (Complex Adsorption and Diffusion Simulation Suite). During our simulations, the *n*-alkane molecules were represented using a flexible united-atom (UA) model where each carbon center and its associated hydrogen atoms were treated as one single Lennard-Jones (LJ) center. The interactions involving these LJ centers were described by the TRAPPE forcefield widely used in simulation studies.[45] For the MOF materials studied here, an atomistic representation was adopted to model all of them. The interactions between alkane molecules and these MOFs were also only described by LJ potential. As done in our previous work,[46] the set of LJ parameters for describing these porous solid frameworks was created by combining the generic UFF interatomic potentials[42] for describing the inorganic part of the crystalline lattice (the metal center with its oxygen environment) and the Dreiding forcefield.[47] During the calculations, all of the structures obtained for the MIL-53(Fe)/alkane pairs were treated as rigid, and periodic boundary conditions were used in the three dimensions. The simulation boxes consisted of 16 (2 × 2 × 4) and 32 (2 × 4 × 4) unit-cells for the NP and LP forms, respectively. The short-range LJ interactions were estimated using a cutoff distance fixed at 12 Å.

Furthermore, in our CB-GCMC simulations, as previously described,[48] the *n*-alkane molecules were grown segment by segment avoiding overlap, and the rules for acceptance or rejection of a grown molecule are selected in a way that they exactly remove the bias caused by this growing scheme. For each state point, the CB-GCMC simulations consisted of 1×10^7 Monte Carlo cycles to guarantee equilibration followed by 1×10^7 cycles to sample the desired thermodynamic properties. In each cycle, one molecule was randomly selected from the system, and the following trial moves were also randomly selected according to the corresponding fixed probabilities mentioned below: (i) displacement (0.1), (ii) rotation around the center of mass (0.1), (iii) partial and full regrowth at random position (both 0.1), and (iv) exchange with the reservoir (0.6). The maximum translational and rotational displacements were adjusted to achieve an acceptance probability of 50%. In addition, the adsorption enthalpies for all alkanes/modified MIL-53(Fe) pairs were computed at low coverage in the NVT ensemble at 303 K using the method recently suggested by Vlugt et al.[49]

RESULTS AND DISCUSSION

Adsorption of C1−C4 Gases and C6−C9 Vapors: Isotherms and XRPD. The adsorption isotherms for the C1−C4 and C6−C9 series for the nonmodified MIL-53(Fe) as well as the functionalized Br, Cl, and CH_3 substituted forms of MIL-53(Fe) are shown in Figures 2−5 and S2 in the case of the NH_2 analogue. The adsorption isotherms for the functionalized materials MIL-53(Fe)-Br, -Cl, -CH_3 exhibit substeps corresponding to a breathing effect upon adsorption as is shown below. These steps are similar to those observed previously for C1−C4 alkanes in MIL-53(Fe), and C1−C9 alkanes in MIL-53(Cr, Al).[15,20] In the case of the nonmodified material MIL-53(Fe)-4H, only the C1−C4 and the C6 adsorbates are adsorbed in significant amounts.[14]

A rapid comparison between the isotherms of the modified and the nonmodified MIL-53(Fe) indicates that introduction of a single functional group on the linker lowers the pressure of each

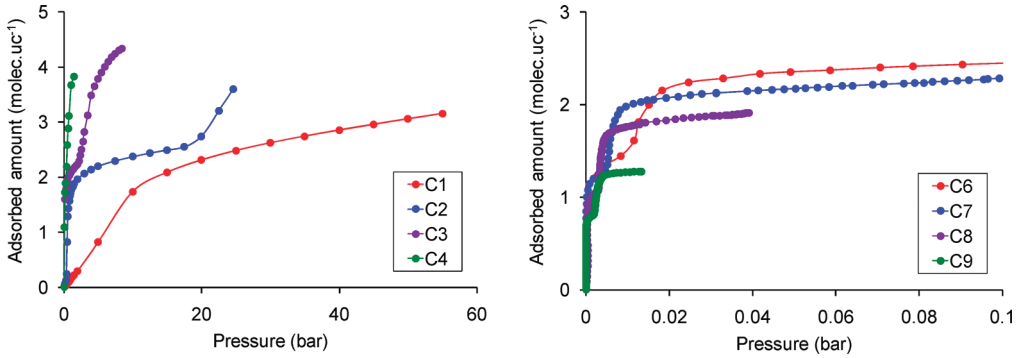

Figure 3. Isotherms for C1−C4 gases (left) at 303 K and C6−C9 vapors at 313 K (right) adsorbed on MIL-53(Fe)-Br.

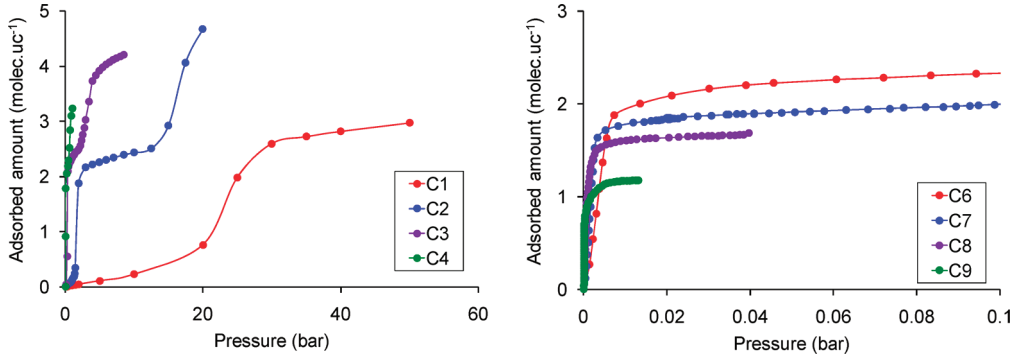

Figure 4. Isotherms for C1−C4 gases at 303 K (left) and C6−C9 vapors at 313 K (right) adsorbed on MIL-53(Fe)-Cl.

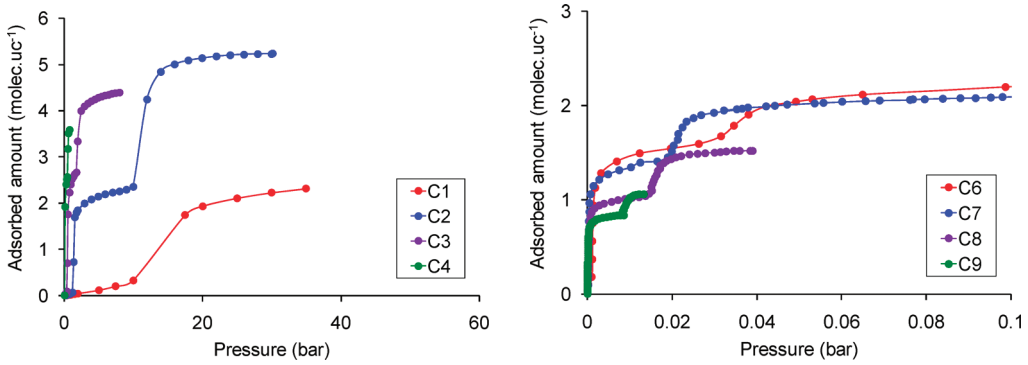

Figure 5. Isotherms for C1−C4 gases at 303 K (left) and C6−C9 vapors at 313 K (right) adsorbed on MIL-53(Fe)-CH_3.

uptake, particularly when the size of the alkyl chain increases. For alkane vapors, adsorption within the nonmodified MIL-53(Fe) is difficult, with a wide pressure induction domain required in the case of C6 before quantitative adsorption takes place. The sigmoïdal shape of this sorption isotherm has already been seen in flexible MOFs and explained by Kitagawa et al.[6] In the case of the C7−C9 vapors, very low total adsorbed amounts have been determined. These can be associated with adsorption isotherms typical of solids with extremely low surface areas.

In their activated forms, all of the MIL-53(Fe) analogues (modified and nonmodified) adopt a closed pore configuration, as reported in a recent study.[35] The cell volume, as well as the size of the pore opening, slightly depend on the nature of the substituent, following the order 4H < NH_2 < Cl < CH_3 < Br. This was attributed to a combination of steric effects and intraframework interactions. Thus, if for short alkanes, this does not make any significant difference, except for the position of the substeps that vary with the nature of the functional group, this is different with longer alkanes, whereas diffusion of the guest species along the pore channels might become harder for MIL-53(Fe) (Figure 2). The increased accessible pore size of the modified MIL-53(Fe) solids (in the closed pore form) thus "solves" this adsorption issue with, as a result, standard adsorption isotherms for such flexible solids, quite similar to those of the MIL-53(Cr, Al) solids.

As shown before, the *n*-alkane adsorption process in the MIL-53(Fe)-X structures also leads to structural changes. In light of the results of C1−C4 adsorption in MIL-53(Fe), where it was shown that the structural change takes place via intermediate

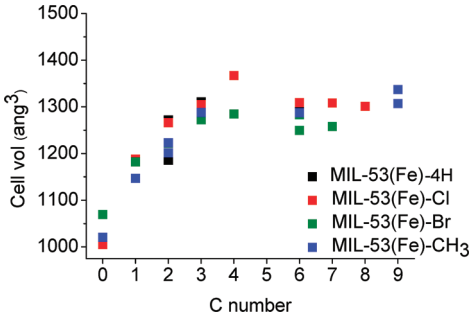

Figure 6. Unit-cell volume of the narrow pore form of the MIL-53(Fe) and the Cl, Br, and CH_3 analogues versus the number of carbon atom in the adsorbed *n*-alkanes.

structures not seen in the case of the Al- and Cr-based materials, either in situ or ex situ (see Experimental Details) X-ray powder diffraction experiments (XRPD) were carried out, depending on the alkane lengths.

Clear-cut correlations between XRPD and adsorption isotherms indicate that for the MIL-53(Fe)-Cl, -Br, -CH_3 materials, three forms are present at the different stages of the adsorption process: the closed pore, the narrow pore, and the large pore forms, and cell parameters are summarized in Tables 1−3, together with their corresponding pressure range of existence. As one might expect, the pressures at which the substeps occur depend on the alkane under consideration as well as on the substituent on the organic linker.

The amounts adsorbed for C1 are larger for the modified MIL-53(Fe)-X materials than for the nonmodified one.[14] In all cases, adsorption of C1 occurs first on the external surfaces of the MOF crystallites, with the solids remaining in their closed pore forms (see Figures 2−5). The pressure required to adsorb C1 within the pores, which occurs through a closed pore−narrow pore transition, nevertheless depends on the functional group, with the value obtained for Br being smaller (1 bar) than those observed for Cl (15−20 bar) and CH_3 (10 bar). This is at a first glance surprising, as our previous studies[35] concluded that the halogenated materials are more difficult to open than the MIL-53(Fe)-CH_3, when considering the halogen−μ_2-OH intraframework interactions, thus requiring framework−guest interactions to open the pores.[35] This could indicate stronger host−guest interactions in the case of MIL-53(Fe)-Br and -Cl than in MIL-53(Fe)-CH_3. However, the pore opening (associated with the *b* cell parameter) is slightly larger for the Br than the other solids in their closed pore forms, which would make it easier for the first molecule to penetrate at the external surface, interact with the pore wall, and set the pore opening process in motion, leading to a lower pressure required to open the closed pore (see below the kinetics studies with C4).

The initial uptake occurs in the same pressure domain for the nonmodified[14] MIL-53(Fe) and the MIL-53(Fe)-CH_3 material (13 bar against 20 bar, respectively). This is associated with the appearance of the triclinic intermediate form with one-half of the pores remaining closed (see Figure 1) for the nonmodified solid,[14] while the narrow pore form (monoclinic, all of the pores slightly open) is directly observed for the modified ones. This could be due to the bulkiness of the substituents, which prevents the formation of a phase with two types of pore aperture.

Furthermore, the uptake of gas adsorbate molecules occurs over a pressure range of 10−15 bar depending on the material and is subsequently followed by a plateau that is usually not completely horizontal, which indicates that the structure continues to change, as shown by the in situ XRPD (see Figures 8 and S3−S21). XRPD indicates that this initial uptake marks the opening of the closed pores (monoclinic *C*2/*c*) toward the narrow pore structure (monoclinic *C*2/*c*), with the latter being the major component of the system when one reaches the plateau (Tables 1−3). In all three cases, the isotherms indicate no further significant uptake of C1 after the first plateau, even at a pressure of 40 bar, showing that this adsorbate cannot fully open neither the MIL-53(Fe)-4H nor the MIL-53(Fe)-X (X = NH_2, Cl, Br, CH_3) materials beyond the narrow pore at the temperature and pressures studied.

The adsorption isotherm curves for the rest of the adsorbates (C2−C4 gases and C6−C9 vapors) also show for the MIL-53(Fe)-X (X = Cl, Br, CH_3) materials an initial region where very little gas or vapor is adsorbed, followed by a short domain of pressure during which there is a steady adsorption, as per the C1 adsorbate. This is followed by a plateau and finally a second step at higher pressure, either fully or partially visible, corresponding to the closed pore−narrow pore and to the narrow pore−large pore transitions at low and high pressure, respectively. As shown before for C1−C4 adsorption on the MIL-53(Fe)-4H material, the pressure at which the closed pore structure begins to open decreases with increasing alkyl chain length of the adsorbate. Once again, as for the C1 adsorbate, the first transition pressure is lower for MIL-53(Fe)-Br than for the other two analogues, and these pressures are similar between the MIL-53(Fe)-Cl and MIL-53(Fe)-CH_3, demonstrating an effect inherent to the material rather than the adsorbate.

After the initial period of low adsorption, the isotherm slopes measured for each adsorbate during the steady adsorption process are almost vertical at very low pressure, regardless of the substituent on the organic linker, which is often interpreted as a result of the high affinity of the pores for the alkanes. The plateau observed after this period of high uptake occurs at decreasing adsorbed quantities with increasing length of the alkane molecules. This plateau is then followed by a second strong uptake of adsorbates (C2−C4 gases and C6−C9 vapors), and the pressure at which this uptake begins increases with decreasing alkyl chain length (Table 1). Finally, in some cases, notably the C6−C9 series, the second plateau, associated with the large pore form, is visible in the isotherm curve. Although this plateau is not seen for the gaseous C1−C4 cases, one can assume that they should be visible if further experiments were to be performed at higher pressures or at lower temperatures. This first plateau spans a domain of pressure, which decreases in size with increasing adsorbate molecule length (see Table S1 for the values), suggesting that any structural change in the framework may be induced more easily using longer chain alkanes. In the case of C2 in MIL-53(Fe)-CH_3, the pressure range is similar to that observed in the nonmodified MIL-53(Fe); however, the case of the latter corresponds to the first intermediate and not the narrow pore form. Therefore, this implies that a similar amount of pressure (thus a similar amount of force) is required to open the first intermediate pore from of MIL-53(Fe) and the narrow pore form of MIL-53(Fe)-CH_3.

If one considers the evolution of the unit-cell volume of the narrow pores form, a clear increase occurs from C1 to C3, followed by a plateau from C4 to C9 (Figure 6). As the volume of the narrow pore form is known to be sensitive to the volume of the entrapped guests,[14,15] it suggests that all of the long *n*-alkanes

(>C3) adopt a similar arrangement within the pores, certainly with the chains lying parallel to the pore axis. This is in full agreement with the fact that the amount of alkane adsorbed in the narrow pore form decreases with increasing number of carbon atoms on the adsorbate.

One can still note that for a given alkane, depending on the experiment and/or the pressure, some variation in the volume of the narrow pore form occurs (see, for example, the case of C2 and C9 in MIL-53(Fe)-CH_3 in Figure 6 and Table 3). This phenomenon was already observed with MIL-53(Cr) and long linear alkanes (C6−C9)[50] and is related to further adsorption/desorption of guests (associated with a slight increase on the intermediate plateau of the isotherm), but could also be associated with a structural rearrangement of the alkanes within the pores.

In all cases, the narrow to large pore transitions occur more easily in the modified materials because the pressure at which the second uptake begins (see Table 3) is lower than those shown for C3 and C4 in the nonmodified material. Thus, one effect of modifying the MIL-53(Fe) material with Cl, CH_3, or Br substituents on the adsorption of *n*-alkanes is that the forces required to initiate the various structural transitions are lower, relative to the nonmodified material. This effect obviously depends on the nature of the substituent. Indeed, the adsorption of these alkanes on an electron-withdrawing substituted material such as MIL-53(Fe)-NH_2 (see Figure S2) does not lead to the structural change, the structure remaining in its closed pore form. As for the adsorption of C7−C9 on the MIL-53(Fe)-4H solid, only a very limited adsorption occurs, most probably on the external surfaces of the MOF crystals.

If for the MIL-53(Fe)-4H solid it is assumed that for longer alkanes the absence of adsorption is likely to be related mostly to diffusion considerations, the case of MIL-53(Fe)-NH_2 shows that the interactions between the alkanes and this particular analogue are not sufficiently strong to overcome the intraframework interactions (hydrogen bonds, in the present case),[35] and thus bring about the structural change. It is also possible that other factors (steric, kinetic, etc.) do not favor the structural transition.

At high pressure, the adsorbed amounts do not differ significantly between the modified Cl, Br, and CH_3 materials regardless of the guest, from C2 to C7, in agreement with the presence of a large pore form, whose volume is almost insensitive to the nature of the alkane and the organic substituent. For the longer alkane vapors (C8 and C9), this observation remains true for the MIL-53(Fe)-Br/Cl, while the amount adsorbed is slightly lower in the MIL-53(Fe)-CH_3. As mentioned in the Experimental Details, this observation has been verified by different sorption experiments using fresh samples of MIL-53(Fe)-CH_3, highlighting the role of steric factors in this material, previously mentioned in the case of a 4CH_3-modified MIL-53(Cr).[51,52]

Kinetic Aspects of the Sorption Processes. Kinetic aspects are of utmost importance in many adsorption/separation processes and could have a strong effect on the adsorption using MIL-53(Fe)-X series of flexible solids.

For each point of the sorption isotherms, the time required for the pressure change to reach zero was recorded during the sorption process, signifying that a static equilibrium had been reached (see Experimental Details). As in our previous study,[15] we focus on the kinetic differences between C6 and C9 in the following discussion, because from previous experience, the adsorption of the C9 molecules is different as compared to the shorter C6−C8 alkanes, an effect that is seen when considering the mass adsorbed rather than the number of molecules (discussed later in this Article). On the corresponding sorption isotherms, the equilibration time was plotted for each point of the isotherms versus the relative pressure. These data can be found in Figure 7 as a typical illustration for the MIL-53(Fe)-Br sample, and in the Supporting Information for the other modified materials (Figures S4,S5).

Different points can be emphasized. For a given material, the equilibration times are longer in the case of the sorption of C6 as compared to that of C9, which has also been demonstrated previously.[15] The models show that in the case of the large pore form the C9 molecule is more likely to be aligned along the *c*-axis of the pores, whereas C6 may be aligned along the *ac*-axis, which can have an effect on the diffusion times and hence the equilibration times.

The general features of the curves are similar between the −Br- and −CH_3-substituted materials. At low relative pressures, a peak is observed, which corresponds to the filling of the narrow pore structure during or after the closed to narrow pore transition, which is consistent with an increase in the space available in which adsorbates may diffuse and arrange themselves more quickly within the pores. A sharp decrease in equilibration times is then observed at increasing relative pressures, corresponding (i) to adsorption on the plateau corresponding to narrow pore form, which prevents the rearrangement of the already adsorbed species, and (ii) to the adsorption of a small amount of alkane in a quasi saturated phase. As the pressure further increases, a second peak in equilibration time appears, which corresponds to the narrow to the large pore transition, for the same reasons as the one previously mentioned. As mentioned above, adsorption of C6−C9 species in the MIL-53(Fe)-4H does not occur within the pores, in contrast to the results obtained for the C1−C4 molecules in the same material.[14] Because the shorter adsorbates fulfill the energetic criteria for the pore opening, it is likely that the C6−C9 molecules would also fulfill this requirement (see the molecular modeling section). This shows that in this case, the kinetics of the process does not favor adsorption of the longer alkanes, an effect related to the different sizes of the closed pore apertures between the nonmodified and modified structures.

These general features are not observed in the case of MIL-53(Fe)-Cl material. In this particular case, the smaller size of the narrow pore plateau renders the flexible character almost invisible of the isotherm, although evidenced by XRPD. It is therefore very difficult to distinguish kinetic transitions in the course of the sorption isotherm. One can only mention an increase of equilibration time as the pores are being filled by the adsorbate followed by a decrease as soon as the saturation plateau is reached.

To evaluate the effect of the functionalization on the ease of the pore opening, activated samples of the MIL-53(Fe) Cl and Br analogues were exposed directly to a high pressure of C4, corresponding to the second plateau (and thus the large pore form), and submitted to XPRD. Both solids present the closed pore to narrow pore and narrow pore to large pore transitions, but the transition occurs more quickly for the Br than the Cl analogue. Although the time needed to switch from the closed to the narrow pore is of the same order of magnitude for both solids (30 and 60 min for Br and Cl, respectively), the effect on the second transition from the narrow to the large pore is more pronounced (45 and 220 min for Br and Cl, respectively) (see Figure 8). Although these measurements are not quantitative, as some experimental factors could change from one experiment to the other (such as the amount of solid), it nevertheless illustrates

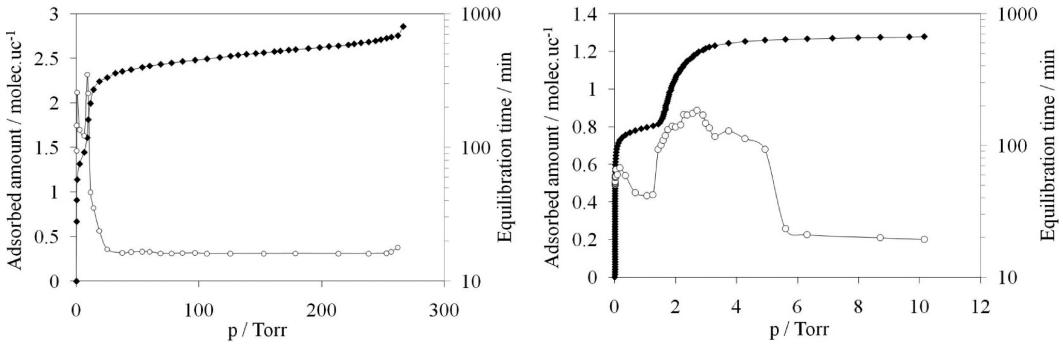

Figure 7. Adsorption of *n*-hexane (left) or *n*-nonane (right) on MIL-53(Fe)-Br at 313 K. Filled symbols correspond to the sorption isotherms, while the empty symbols correspond to the equilibration time for each data point of the sorption isotherm.

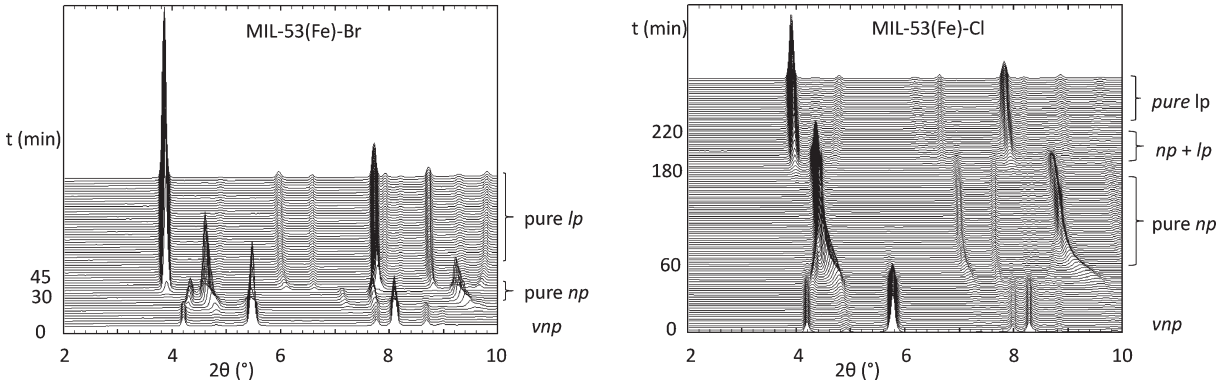

Figure 8. Adsorption of C4 in MIL-53(Fe)-Br (left) and MIL-53(Fe)-Cl (right). The pressure was fixed to 3.2−3.1 and 2.8−2.7 bar, respectively.

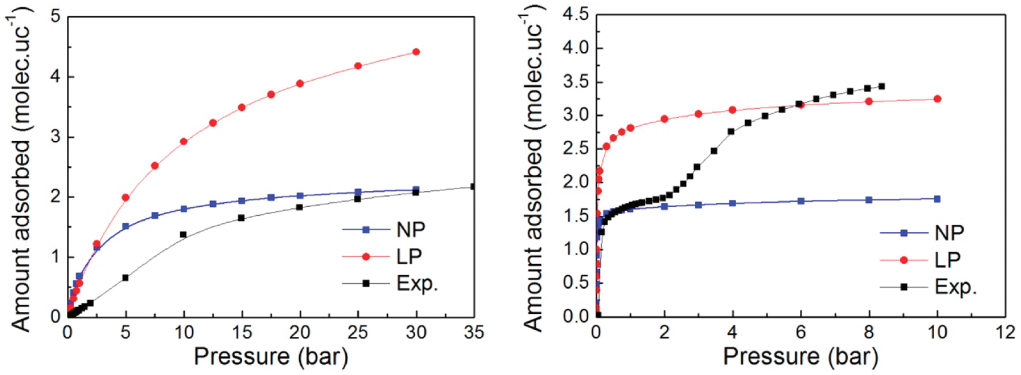

Figure 9. Comparison of the experimental and the calculated isotherms in the narrow and large pore forms for C1 (left) and C3 (right) in MIL-53(Br).

clearly the gain in terms of rate of adsorption of the organic functionalization. The same effect could be expected in other gate opening systems.

Insights from Molecular Simulations: Adsorption Isotherms and Enthalpies. To gain further insight into the phenomena demonstrated by our experiments, Configurational Bias GCMC simulations were performed. This also allows the probing of the adsorption enthalpies at zero coverage to obtain a clearer idea of the interactions that take place between the alkanes and the MIL-53(Fe)-X framework.

As a typical illustration, the calculated adsorption isotherms for the C1 and C3 gases, and for the C6 and C8 vapors, for the large and narrow pore forms of the MIL-53(Fe)-Br material are shown in Figures 9 and 10, respectively, along with the comparison with the corresponding experimentally measured isotherm (the rest of the simulated isotherms are available in the Supporting Information). As in previous computational studies of adsorption in flexible MOFs,[11] each simulated isotherm is assigned to a region on the experimental isotherm, thus corroborating the experimental evidence and interpretations with regards to which structure is present during the adsorption process.

For all of the molecules under consideration, the simulated adsorption isotherm for the narrow pore form broadly corresponds to the initial region of the experimental isotherms up to the end of the first plateau in terms of adsorbed amount. Nevertheless, XRPD indicates that, for a solid/adsorbate pair, the volume of the

dx.doi.org/10.1021/jp205369t |*J. Phys. Chem. C* 2011, 115, 18683–18695

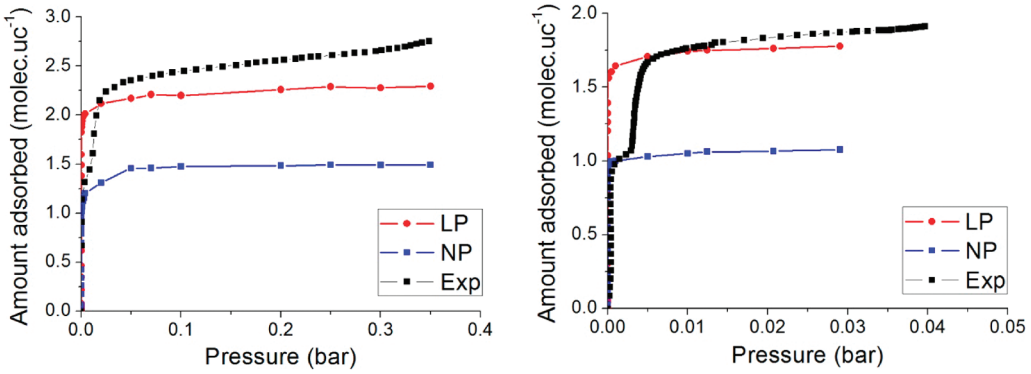

Figure 10. Comparison of the experimental and the calculated isotherms in the narrow and large pore forms for C6 (left) and C8 (right) in MIL-53(Br).

narrow pore slightly changes on the plateau (see above and Tables 1−3). This behavior is not taken into account here, because a simulation cell of fixed volume is used and may lead to slight discrepancies between experimental and simulated isotherms. Another source of error lies in the structural model itself. In the experimental structure, the functional group distribution is disordered on the phenyl ring. However, in our model, the distribution is ordered. Therefore, although one can predict which pore form might dominate at a given point in the isotherms, the dimensions of the pore in the model do not necessarily match that of the pore present at the same point in the experimental isotherm. This complexity of the system is evident from our simulated isotherms, because depending on the adsorbate under consideration (as well as the material), one can see from the simulated curves that the plateaus are predicted with some uncertainty.

For the shorter, gaseous alkanes (C1−C4), with which it is relatively difficult to open the closed pore form, a larger portion of the initial part of the isotherms (i.e., up to the first plateau) might be due to the progressive nature of the transition from the closed to the narrow pore versions. As the alkane molecules increase in length (going above C4, toward C9), isotherms indicate that the pores open more easily (at lower pressures), regardless of the MIL-53(Fe)-X form at hand. It should be noted that in the C1 case, the simulated isotherm for the large pore form only gives a theoretical indication of the amount of C1 that could be adsorbed in a large pore of the relevant MIL-53-(Fe)-X analogue, because the large pore is not is observed experimentally for C1.

The simulated isotherms (C2−C9) for the large pore structures correspond broadly to the second substep on the experimental adsorption isotherms in terms of the amounts absorbed. However, analysis of the simulated curves shows that the GCMC calculations do not match the experimental isotherm curves. An explanation is that a phase mixture comprising the narrow and large pore forms exists in the system, as indicated by the X-ray diffraction studies described earlier in this Article. Thus, it is also likely that some narrow pores remain, resulting in discrepancies between the simulations and the experiments.

In the case of C6−C9 in the MIL-53(Fe)-Cl material, we have already described the isotherm as being of the IUPAC-defined type 1 in terms of its overall shape, although the structural change described here does occur for this material upon adsorption of C1−C9 alkanes in the same manner as the other two MIL-53(Fe)-X analogues. The same problem was found for the MIL-53(Cr)/C2 system and related to the weaker sensitivity of the isotherm (a value averaging all of the pore openings is measured) when compared to XRPD (all of the phases are seen separately).[20] The absence of the first substep in the C6−C9 isotherms makes the determination of the pressure at which the narrow to large pore transition occurs difficult. However, our simulated isotherms can give an idea of where the transition occurs by considering the amount that could be adsorbed in a narrow pore structure of the MIL-53(Fe)-Cl (see Figure 11) and coupling this with the kinetic data already discussed above. The saturation plateau calculated for this structure is 1.5 molecules per unit-cell in the case of C6 and 1 molecule/u.c. for the C7, C8, and C9 cases. The relative pressure at which these adsorbed amounts are reached is shown to be between 0.01 and 0.02.

The kinetic data for the cases C6 and C9 in MIL-53(Fe)-Cl show a peak at a relative pressure right after the point that the simulations show that saturation of the narrow pore structure is achieved. This peak corresponds to a narrow to large pore opening and indicates that equilibrium of the system is at its lowest due to the diffusion of the molecules and their subsequent rearrangement in the large pore phase. This shows that the closed to narrow to large pore transition occurs in a closed pressure range.

The role of the adsorption enthalpy gives further insight into the adsorption process as well as a rationalization of experimental phenomena. The values of the simulated enthalpies at zero coverage for the narrow pore form are shown in Figure 12. The enthalpies, which vary between −18 and −106 kJ/mol, from C1 to C9, are very similar between the different analogues, although a general trend is observed with the enthalpies following the order $-CH_3$ < −Cl < −Br. One can also see a linear evolution of the enthalpies with increasing chain length, which corresponds to the addition of a $-CH_2$ group to the alkyl chain, This linear evolution of the enthalpy has already been demonstrated in the case of adsorption of the shorter alkanes (C1−C4) in the MIL-53(Cr, Fe) and the MIL-47(V) materials.[46,50] The corresponding slopes of −10 kJ mol^{-1} for the −Br and −Cl forms and −8 kJ mol^{-1} for the $-CH_3$ version show that the enthalpy contribution is higher for the halogens substituents than for the $-CH_3$ one. This is consistent with the fact that the halogen atoms would in reality perturb the electron clouds on the alkane more than a $-CH_3$ group, thus generating a stronger van der Waals interaction.

The minimum adsorption enthalpy required to induce the large to narrow pore transition in the MIL-53(Cr) material has been proposed to be around −20 kJ/mol.[20] In the case of this study, the process is the opposite, in that the pores only open upon adsorption. One of the interactions that is said to hold the pores closed (for the halogenated materials) is the hydrogen

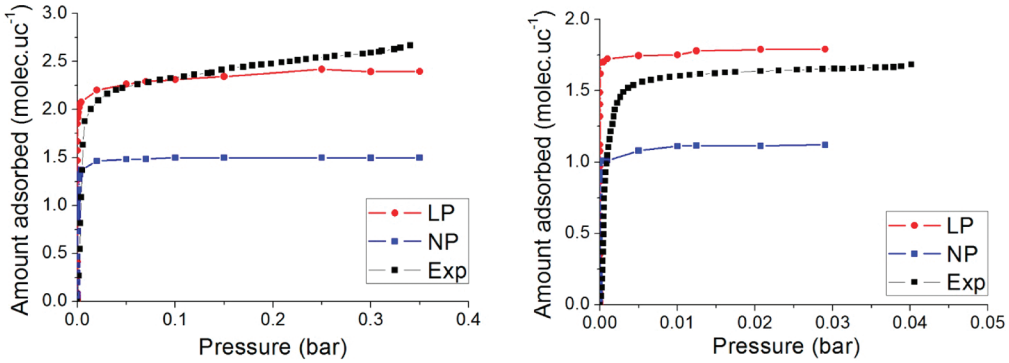

Figure 11. Comparison of the experimental and the calculated isotherms in the narrow and large pore forms for C6 (left) and C8 (right) in MIL-53(Cl).

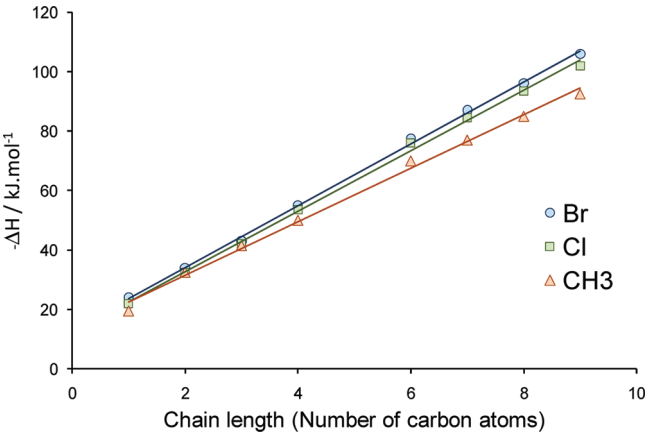

Figure 12. Enthalpies of adsorption obtained by Monte Carlo simulations at the initial stage of loading at 313 K for the NP form of MIL-53(Fe)-X (X = CH_3, Br, Cl) reported as a function of the carbon number.

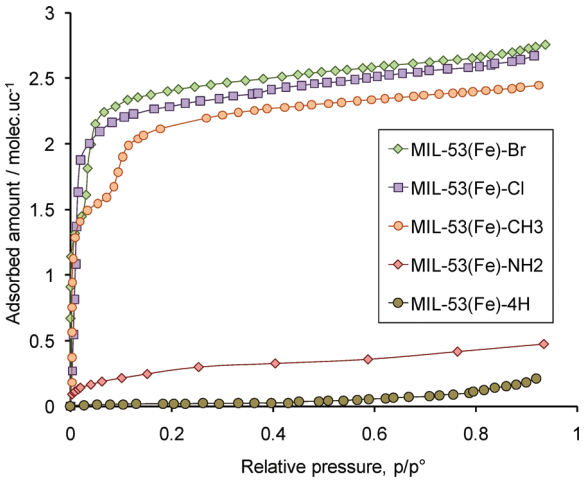

Figure 13. Comparison of the adsorption properties of the modified MIL-53(Fe)-X as compared to the nonmodified analogue (MIL-53(Fe)-4H) in the case of *n*-hexane.

bonds between the μ_2-OH groups and the substituents on the organic linkers, and for pore opening to occur, these interactions would have to be broken or perturbed, by the interaction between the alkane and either the grafted functions or the μ_2-OH groups. However, this only represents part of the story because the other interactions (and their relative strengths) can have an appreciable effect, such as $\pi-\pi$ interactions between the aromatic rings or $-CH-\pi$ interactions (present in all of the analogues presented here).

The occurrence of the pore opening is likely to be related to the balance between van der Waals interaction between sorbate species and pore walls, $\pi-\pi$ interaction between aromatic linkers, and interactions between μ_2-OH groups of the framework and the aromatic linkers.

An example is the case of the nonmodified MIL-53(Fe), which has closed pores that are narrower than in the functionalized analogues. The extent of this perturbation required can be reflected in the values of the enthalpies. For C1, which has an adsorption enthalpy of between −19 and −24 kJ/mol depending on the modified MIL-53(Fe) forms, no narrow to large pore transition is observed. This structural change is seen from the C2 to the C9 cases. The adsorption enthalpies for C2 lie in the range −32 to −34 kJ/mol, with the enthalpies increasing with increasing number of C atoms on the adsorbate. Therefore, a minimum adsorbate−framework interaction energy in the range of −24 to −32 kJ/mol (depending on the material) is probably required at the temperature range between 303 and 313 K to sufficiently perturb the interactions that hold the narrow pore structure closed and initiate the narrow to large pore transition.

The linear relationship between the enthalpy of adsorption and the number of carbon atoms on the adsorbate molecule would imply that the conformations of the molecules at low coverage are very similar, because each new $-CH_2$ group would have to interact with the framework and contribute to the adsorption enthalpy, which would preclude certain conformations. This is in full agreement with the XPRD data that shows that the cell dimensions for narrow pore (Figure 6) are not drastically affected when one goes from C3 to C9.

CONCLUSION

Flexible MOFs are promising adsorbents in many ways, and among this new class of porous materials, the MIL-53(Fe) solids pave the way to the design of adsorbents, which could adsorb selectively from a specific pressure that only depends on temperature and on the nature of adsorbates. This study shows that even nonpolar molecules can induce the structural transition for which the MIL-53(Fe) series are known for, and that, although the iron-containing material is generally difficult to open, substitution on the aromatic rings induces changes (such as forces present in the material) so as to render adsorption within the pores possible, particularly when the size of the adsorbate

increases. This is summarized in Figure 13. The use of functional groups on the organic linkers modifies the behavior of the structures upon adsorption of nonpolar molecules, associated with structural changes (the so-called "breathing effect") whose pressure and ease are different, and depends on both the adsorbate as well as the exact material. The study also shows that the different intermediates through which the structures pass to reach the large pore form are different between the nonmodified and the modified MIL-53(Fe), with the triclinic intermediate form not being seen for the modified materials. An important point is that the flexibility is induced by a complex interplay between several factors. Although the energetic criterion play a central role, the balance between this criterion and the kinetic aspects of the process (for instance, the molecular diffusion) governs the structural changes observed in our experiments.

Further study using DFT methods may provide insight into these changes that take place. In any case, the fact that these adsorbates induce a structural change to the large pore form shows that strong polar interactions are not the only driving force for this phenomenon.

■ ASSOCIATED CONTENT

Supporting Information. Interatomic potentials used in the simulations, MIL-53(Fe)-NH_2 isotherms, crystallographic data obtained from the in situ and ex situ XRPD experiments, as well as all of the simulated adsorption isotherms (as compared to the experimental data). This material is available free of charge via the Internet at http://pubs.acs.org.

■ AUTHOR INFORMATION

Corresponding Author

*Tel.: 0033467163484. Fax: 0033467163470. E-mail: philippe.trens@enscm.fr.

■ ACKNOWLEDGMENT

This work was funded by a French ANR grant (ANR-07-BLAN-0284-02-SAHFS). Florence Ragon is thanked for the synthesis of MIL-53(Fe)-NH_2.

■ REFERENCES

(1) Férey, G. *Chem. Soc. Rev.* **2008**, *37*, 191.
(2) Rowsell, J. L. C.; Yaghi, O. M. *Microporous Mesoporous Mater.* **2004**, *73*, 3.
(3) Kitagawa, S.; K., R.; Noro, S. *Angew. Chem., Int. Ed.* **2004**, *43*, 2334.
(4) McKinlay, A. C.; Morris, R. E.; Horcajada, P.; Férey, G.; Gref, R.; Couvreur, P.; Serre, C. *Angew. Chem., Int. Ed.* **2010**, *49*, 6260.
(5) Serre, C.; Mellot-Draznieks, C.; Surblé, S.; Audebrand, N.; Fillinchuk, Y.; Férey, G. *Science* **2007**, *315*, 1828.
(6) Tanaka, D.; Nakagawa, K.; Higuchi, M.; Horike, S.; Kubota, Y.; Kobayashi, T. C.; Takata, M.; Kitagawa, S. *Angew. Chem., Int. Ed.* **2008**, *47*, 3914.
(7) Serre, C.; Millange, F.; Noguès, M.; Thouvenot, C.; Marsolier, G.; Louër, D.; Férey, G. *J. Am. Chem. Soc.* **2002**, *124*, 13519.
(8) Loiseau, T.; Serre, C.; Huguenard, C.; Fink, G.; Taulelle, F.; Henry, M.; Bataille, T.; Férey, G. *Chem.-Eur. J.* **2004**, *10*, 1373.
(9) Serre, C.; Bourrelly, S.; Vimont, A.; Ramsahye, N. A.; Maurin, G.; Llewellyn, P. L.; Daturi, M.; Filinchuk, Y.; Leynaud, O.; Barnes, P.; Férey, P. *Adv. Mater.* **2007**, *19*, 2246.
(10) Bourrelly, S.; Llewellyn, P. L.; Serre, C.; Millange, F.; Loiseau, T.; Ferey, G. *J. Am. Chem. Soc.* **2005**, *127*, 13519.
(11) Ramsahye, N. A.; Maurin, G.; Bourrelly, S.; Llewellyn, P.; Loiseau, T.; Devic, T.; Serre, C.; Férey, G. *Chem. Commun.* **2007**, 3261.
(12) Coudert, F. X.; Mellot-Draznieks, C.; Fuchs, A. H.; Boutin, A. *J. Am. Chem. Soc.* **2009**, *131*, 11329.
(13) Coombes, D. S.; Cora, F.; Mellot-Draznieks, C.; Bell, R. G. *J. Phys. Chem. C* **2009**, *113*, 544.
(14) Llewellyn, P. L.; Horcajada, P.; Maurin, G.; Devic, T.; Rosenbach, N.; Bourrelly, S.; Serre, C.; Vincent, D.; Loera-Serna, S.; Filinchuk, Y.; Férey, G. *J. Am. Chem. Soc.* **2009**, *131*, 13002.
(15) Trung, T. K.; Trens, P.; Tanchoux, N.; Bourrelly, S.; Llewellyn, P. L.; Loera-Serna, S.; Serre, C.; Loiseau, T.; Fajula, F.; Férey, G. *J. Am. Chem. Soc.* **2008**, *130*, 16926.
(16) Ghoufi, A.; Maurin, G.; Férey, G. *J. Phys. Chem. Lett.* **2010**, *1*, 2810.
(17) Vimont, A.; Travert, A.; Bazin, P.; Lavalley, J.-C.; Daturi, M.; Serre, C.; Férey, G.; Bourrelly, S.; Llewellyn, P. L. *Chem. Commun.* **2007**, 3291.
(18) Coudert, F. X.; Boutin, A.; Jeffroy, M.; Mellot-Draznieks, C.; Fuchs, A. H. *ChemPhysChem* **2011**, *12*, 247.
(19) Férey, G.; Serre, C.; Devic, T.; Maurin, G.; Jobic, H.; Llewellyn, P. L.; De Wiereld., G.; Vimont, A.; Daturi, M.; Chang, J.-S. *Chem. Soc. Rev.* **2011**, *40*, 550.
(20) Llewellyn, P. L.; Maurin, G.; Devic, T.; Loera-Serna, S.; Rosenbach, N.; Serre, C.; Bourrelly, S.; Horcajada, P.; Filinchuk, Y.; Férey, G. *J. Am. Chem. Soc.* **2008**, *130*, 12808.
(21) Liu, Y.; Her, J. H.; Dailly, A.; Ramirez-Cuesta, A. J.; Neumann, D. A.; Brown, C. M. *J. Am. Chem. Soc.* **2008**, *130*, 11813.
(22) Walker, A. M.; Civalleri, B.; Slater, B.; Mellot-Draznieks, C.; Cora, F.; Zicovich-Wilson, C. M.; Roman-Perez, G.; Soler, J. M.; Gale, J. D. *Angew. Chem., Int. Ed.* **2010**, *49*, 7501.
(23) Neimark, A. V.; Coudert, F.-X.; Boutin, A.; Fuchs, A. H. *J. Phys. Chem. Lett.* **2010**, *1*, 445.
(24) Beurroies, I.; Boulhout, M.; Llewellyn, P. L.; Kuchta, B.; Férey, G.; Serre, C.; Denoyel, R. *Angew. Chem., Int. Ed.* **2010**, *49*, 7526.
(25) Millange, F.; Guillou, N.; Walton, R. I.; Grenèche, J.-M.; Margiolaki, I.; Férey, G. *Chem. Commun.* **2008**, 4732.
(26) Devautour-Vinot, S.; Maurin, G.; Henn, F.; Serre, C.; Devic, T.; Férey, G. *Chem. Commun.* **2009**, 2733.
(27) Rowsell, J. L. C.; Millward, A. R.; Park, K. S.; Yaghi, O. M. *J. Am. Chem. Soc.* **2004**, *126*, 5666.
(28) Rowsell, J. L. C.; Yaghi, O. M. *J. Am. Chem. Soc.* **2006**, *128*, 1304.
(29) Hasegawa, S.; Horike, S.; Matsuda, R.; Furukawa, S.; Mochizuki, K.; Kinoshita, Y.; Kitagawa, S. *J. Am. Chem. Soc.* **2007**, *129*, 2607.
(30) Boutin, A.; Couck, S.; Coudert, F.-X.; Serra-Crespo, P.; Gascon, J.; Kapteijn, F.; Fuchs, A.; Denayer, J. F. M. *Microporous Mesoporous Mater.* **2011**, *140*, 108.
(31) Couck, S.; Remy, T.; Baron, G. V.; Gascon, J.; Kapteijn, F.; Denayer, J. F. M. *Phys. Chem. Chem. Phys.* **2010**, *12*, 9413.
(32) Gascon, J.; Aktay, U.; Hernandez-Alonso, M. D.; van Klink, G. P. M.; Kaptejin, F. *J. Catal.* **2009**, *261*, 74.
(33) Torrisi, A.; Bell, R. G.; Mellot-Draznieks, C. *Cryst. Growth Des.* **2010**, *10*, 2839.
(34) Ghosh, S. K.; Bureekaew, S.; Kitagawa, S. *Angew. Chem., Int. Ed.* **2008**, *47*, 3403.
(35) Devic, T.; Horcajada, P.; Serre, C.; Salles, F.; Maurin, G.; Moulin, B.; Heurtaux, D.; Clet, G.; Vimont, A.; Greneche, J.-M.; Ouay, B. L.; Moreau, F.; Magnier, E.; Filinchuk, Y.; Marrot, J.; Lavalley, J.-C.; Daturi, M.; Férey, G. *J. Am. Chem. Soc.* **2010**, *132*, 1127.
(36) Llewellyn, P. L.; Maurin, G. *C. R. Chim.* **2005**, *8*, 283.
(37) De Weireld, G.; Frere, M.; Jadot, R. *Meas. Sci. Technol.* **1999**, *10*, 117.
(38) Tanchoux, N.; Trens, P.; Maldonado, D.; Di Renzo, F.; Fajula, F. *Colloids Surf., A* **2004**, *246*, 1.
(39) Boultif, A.; Louer, D. *J. Appl. Crystallogr.* **1991**, *24*, 987.
(40) Roisnel, T.; Rodriguez-Carvajal, J. *Abstr. 1st European Powder Diffraction Conf.* **1991**, 127.
(41) Roisnel, T.; Rodriguez-Carvajal, J. *Abstr. 7th European Powder Diffraction Conf.* **2000**, 71.

(42) Rappe, A. K.; Casewit, C. J.; Colwell, K. S.; Goddart, W. A., III; Skiff, W. M. *J. Am. Chem. Soc.* **1992**, *114*, 10024.
(43) *Accelrys*; Materials Studio software: San Diego, CA, 2008.
(44) Salles, F.; Maurin, G.; Serre, C.; Llewellyn, P. L.; Knofel, C.; Choi, H. J.; Filinchuk, Y.; Oliviero, L.; Vimont, A.; Long, J. R.; Férey, G. *J. Am. Chem. Soc.* **2010**, *132*, 13782.
(45) Martin, M. G.; Siepmann, J. I. *J. Phys. Chem. B* **1998**, *102*, 2569.
(46) Rosenbach, J. N.; Ghoufi, A.; Deroche, I.; Llewellyn, P. L.; Devic, T.; Bourrelly, S.; Serre, C.; Férey, G.; Maurin, G. *Phys. Chem. Chem. Phys.* **2010**, *12*, 6428.
(47) Mayo, S. L.; Olafson, B. D.; Goddart, W. A., III. *J. Phys. Chem. B* **1990**, *94*, 8897.
(48) Beerdsen, E.; Smit, B.; Calero, S. *J. Phys. Chem. B* **2002**, *106*, 10659.
(49) Vlugt, T. J. H.; García-Pérez, E.; Dubbeldam, D.; Ban, S.; Calero, S. *J. Chem. Theory Comput.* **2008**, *4*, 1107.
(50) Trung, T. K.; Deroche, I.; Rivera, A.; Yang, Q. Y.; Yot, P.; Ramsahye, N.; Vinot, S. D.; Devic, T.; Horcajada, P.; Serre, C.; Maurin, G.; Trens, P. *Microporous Mesoporous Mater.* **2011**, *140*, 114.
(51) Serre, C.; Millange, F.; Devic, T.; Audebrand, N.; van Beek, W. *Mater. Res. Bull.* **2006**, *41*, 1550.
(52) Comotti, A.; Bracco, S.; Sozzani, P.; Horike, S.; Matsuda, R.; Chen, J.; Takata, M.; Kubota, Y.; Kitagawa, S. *J. Am. Chem. Soc.* **2008**, *130*, 13664.